NANO LETTERS

2007
Vol. 7, No. 5
1329−1337

Sub-10 nm Device Fabrication in a Transmission Electron Microscope

Michael D. Fischbein and Marija Drndić*

Department of Physics and Astronomy, University of Pennsylvania, 209 South 33rd Street, Philadelphia, Pennsylvania 19104

Received February 14, 2007; Revised Manuscript Received March 26, 2007

ABSTRACT

We show that a high-resolution transmission electron microscope can be used to fabricate metal nanostructures and devices on insulating membranes by nanosculpting metal films. Fabricated devices include nanogaps, nanodiscs, nanorings, nanochannels, and nanowires with tailored curvatures and multi-terminal nanogap devices with nanoislands or nanoholes between the terminals. The high resolution, geometrical flexibility, and yield make this fabrication method attractive for many applications including nanoelectronics and nanofluidics.

The ability to efficiently fabricate high-quality nanostructured devices is important because many physical, chemical, and biological properties of diverse systems depend on electron motion, fluid motion, and/or chemical reactions that occur at nanometer scales. For instance, electrons typically travel a few nanometers at room temperature before scattering inelastically in metals[1] or flipping their spin in ferromagnetic metals,[2] and their transition into the superconducting phase becomes sensitive to size at ~10 nm.[3−6] Nanometer-scale fluid flow deviates from bulk flow,[7] and water confined in a nanometer-scale volume crystallizes at room temperature.[8] Control over molecular motion in nanometer-wide channels is important for studies of molecular-scale mass transport and for nanofluidic applications in genomics.[9] In pursuing nanoscale science, many different approaches have been undertaken to fabricate the small structures needed to probe the phenomena. The widely used resist-based scanning electron beam lithography techniques are limited down to tens of nanometers and top-down fabrication of sub-10 nm scale devices with high reproducibility and yield is generally still challenging.

In this paper, we demonstrate the use of a transmission electron beam (TEB) to make nanoscale metal devices of arbitrary geometries on insulating platforms. Our technique should additionally facilitate a range of nanoscience applications including nanoelectronics and molecular translocation studies. This new top-down TEB-based method works by controllably ablating evaporated metal films, pre-patterned with electron beam lithography (EBL) on silicon nitride membrane substrates, to produce intricate metal (Ni, Cr, Al, Ag, and Au) nanoscale devices with near-atomic precision. We show a variety of different device geometries (nanoscale gaps, channels, wires, discs, rings, three-, four-, and 8-terminal electronic devices, etc.) with sub-10 nm features with straight and circular segments and we discuss their fabrication, electrical characterization, and applications. These nanostructures are fabricated at precise locations and seamlessly integrated into large-scale circuitry without contact resistance.

This TEB-"ablation lithography" (here referred to as TEBAL) does not require the use of resist or a lift-off step. Furthermore, in situ imaging of metal ablation allows for real-time feedback control and Angstrom-resolution visual inspection of the fabricated devices. Together, these benefits allow for low surface roughness (<5 Å) and high reproducibility of the TEBAL-fabricated nanostructures.

Transmission electron beams (TEBs) have long been used to study materials at nanometer scales. Upon electron irradiation of a sample, high-energy electrons lose a portion of their kinetic energy via inelastic scattering processes in the solid, resulting in various effects including sputtering, amorphization, sublimation, and desorption. These effects have generally been considered unwanted artifacts in the field of electron microscopy. In the late 1970s and early 1980s, Cherns demonstrated that a 1 MeV TEB can induce "transmission sputtering"[10] in Au and proposed a many-body collision model to explain this effect by surface diffusion and agglomeration of surface vacancies.[11,12] This work was followed by other researchers to drill holes and lines in crystalline solids (e.g., quartz[13] and NaCl[14]) and amorphous solids (alumina sheets,[15−17] CaF_2, and MgO[17]). Recent examples include the drilling of nanoholes in silicon,[18] stainless steel,[19] and in Si_3N_4 and SiO_2 membranes.[20,21] TEB-induced atomic rearrangement has been observed in Au piezoelectric point contacts,[22] Au nanoparticles,[23] and free-standing Au nanobridges suspended from Au (001) films.[24] TEBs have been used to observe the sublimation of nano-

* Corresponding author. E-mail: drndic@physics.upenn.edu.

10.1021/nl0703626 CCC: $37.00
Published on Web 04/17/2007

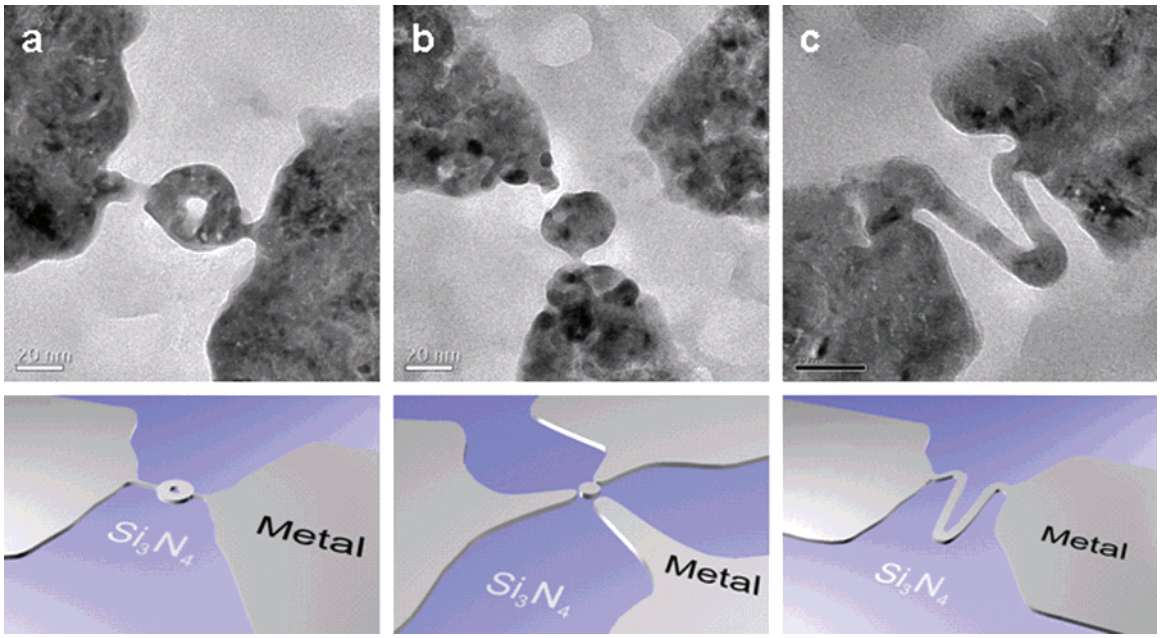

Figure 1. Example structures to demonstrate the flexibility of TEBAL. Each of the three structures shown in the TEM images is accompanied by a schematic (below) showing the fabrication by TEBAL. (a) Nanoring with outer radius of ~18.5 nm and inner radius of ~3 nm (scale = 20 nm). (b) Three-terminal electronic device: source and drain leads are coupled to a ~13 nm radius metallic island and a gate electrode ~23 nm away from the island (scale = 20 nm). The rate-limiting tunneling barrier (upper junction) is a 2.7 nm gap. (c) Serpentine wire with 6 nm width (scale = 20 nm). All lengths were measured with Gatan's Digital Micrograph image analysis software.

meter-scale Ag particles,[25] to melt Al−Si particles,[26] to transform diamond nanoparticles into onion-like carbon,[27] and to reduce SiO_2 to Si.[28] TEB-induced sample modification has recently attracted interest for device fabrication, and some progress has been made in that direction. TEBs have been used to break Au and Pt wires,[29] to join single-wall carbon nanotubes,[30] and to "weld" and inscribe synthesized silicon and metal nanowires on holey carbon grids[31] and suspended on DNA templates.[32]

Here we demonstrate that a TEB can be used to fabricate arbitrary metal nanostructure geometries in two-dimensions (nanowires, nanogaps, nanorings, multi-terminal devices, etc.) without the need for a mask or resist. To illustrate the flexibility of TEBAL, we show in Figure 1 three example structures made from a Ni/Cr alloy: a nanoring (Figure 1a) with inner and outer radii of ~3 and ~18.5 nm, a three-terminal single-electron transistor geometry (Figure 1b), and a serpentine, U-shaped, wire (Figure 1c) with a width of ~6 nm, total length of ~100 nm, and radius of curvature of ~1 nm at the three bends. A corresponding schematic is shown for each structure for clarity. Several stages of carving out the final nanoring in Figure 1a from a metal strip to first form a nanodisc of radius ~22.5 nm and then a nanoring of radius ~19.5 nm are shown in Figure S1 (Supporting Information). Each structure was intentionally left connected to its "parent leads" to demonstrate the ease of their integration into complete circuits. The feature sizes were measured with the same Gatan Digital Micrograph image software that was used to obtain the HRTEM images. The images were not altered or processed in any way after being captured by the CCD camera of the HRTEM (i.e., they are "raw"). The contrast, brightness, and sharpness in the images are exactly as they appear to the user during the fabrication. A detailed analysis of these TEM images is included in the Supporting Information. Post-fabrication, the structures were imaged several times over a period of weeks and displayed no sign of change or "relaxation" into different shapes over time. TEBAL fabrication has the added advantage of maintaining a resistance-free contact between a nanostructure and its leads. This is in contrast to bottom-up (e.g., chemically synthesized) nanostructures, which typically need to be first located on a chip and then contacted to larger circuitry, all after their fabrication.

The TEBAL process is outlined in Figure 2, where we illustrate the fabrication of a ~18 nm diameter Ni/Cr metal disc connected to the parent leads with two short ~4.5 nm wide nanowires. The metal to be nanosculpted by the ablating beam was first pre-patterned by electron beam lithography (EBL) into an ~80 nm wide metal strip on the silicon nitride membrane that is itself essentially transparent to the electron beam. The parallel fabrication of many such membranes is well documented in existing literature.[33,34] We used low-stress amorphous silicon nitride (Si_3N_4) on ~0.5 mm thick p-type silicon (Si^+). The Si_3N_4 is initially 100 nm thick and later etched to be ~40 nm thick via SF_6 reactive ion etching. Each 4 in. Si_3N_4/Si^+ wafer is processed to produce many ~5 × 5 mm^2 square chips each with a 50 × 50 μm^2 region in their center where the Si_3N_4 membrane is freely suspended (Figure S2, Supporting Information). Importantly, these low-stress Si_3N_4 suspended membranes are mechanically robust, their thickness can be controlled by reactive ion etching from several hundreds of nanometers to as low as ~10 nm, and these chips can be easily handled and processed (e.g., spin-casting and EBL) without incurring damage.

The thickness of the EBL pre-patterned metal films ranged from 10 to 50 nm. Metal films were evaporated using

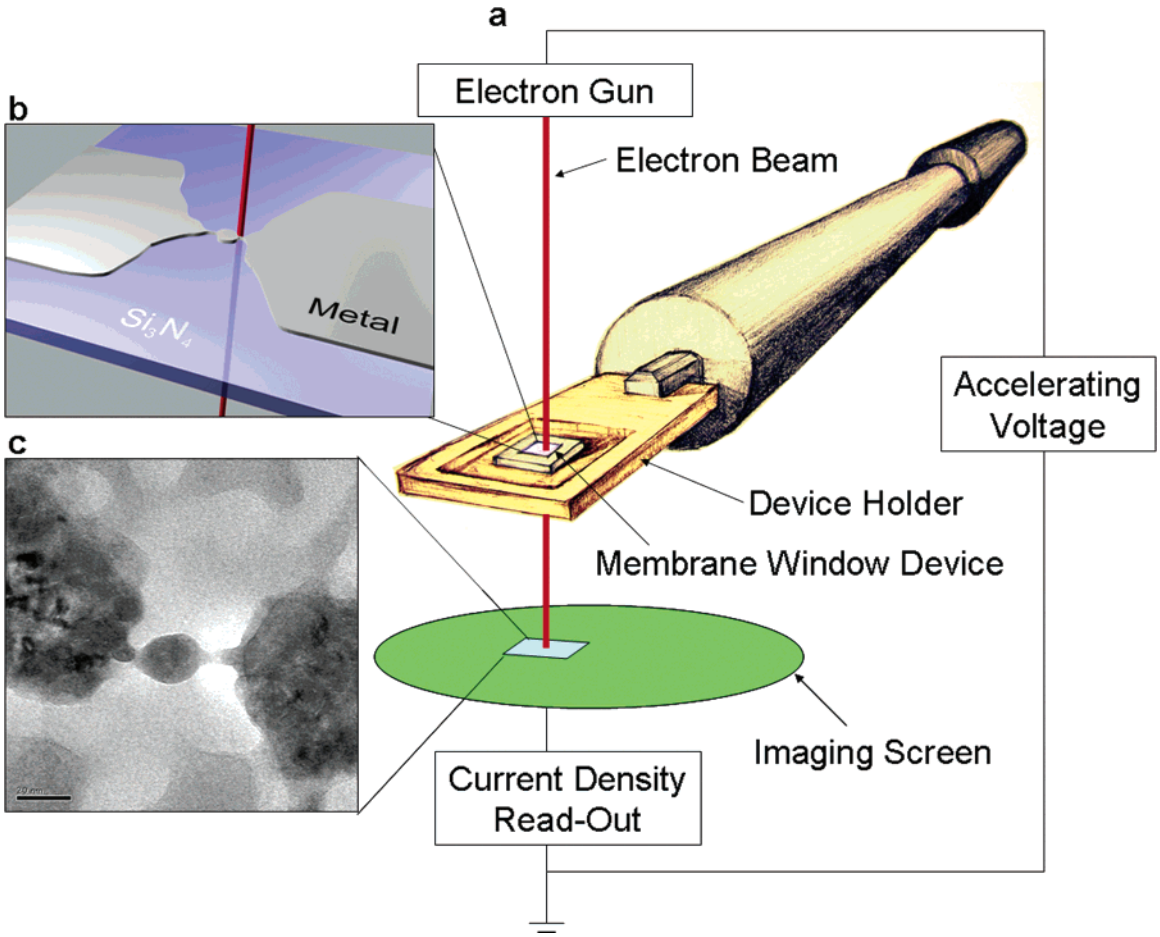

Figure 2. Apparatus for TEBAL. (a) Membrane window device with pre-patterned metal lines on its surface is loaded into the TEM environment. The metallized surface of the membrane faces away from the beam source (i.e., toward the imaging screen). A hole (not shown) in the device holder allows the beam to pass completely through the membrane and reach the imaging screen. (b) Schematic of the ablation of a pre-patterned wire to achieve a metal disk that is connected to the initial metal on both sides. (c) TEM image of an actual 18 nm diameter metallic disk that was nanosculpted from Ni/Cr with TEBAL and left connected to the parent-leads with two ~4.5 nm wide nanowires (scale = 20 nm). The imaging screen enables real-time visual feedback for a user or real-time current density feedback for computerized control.

standard thermal evaporation procedures at a rate ~0.3 nm/s and pressure $<10^{-6}$ Torr. The feature resolution achieved on Si_3N_4 membranes with EBL is enhanced significantly due to the minimization of electron backscattering,[36] and we recently fabricated high-quality nanogaps directly with EBL.[37] It is therefore possible to start with metal features that are already small compared to what is usually achieved with EBL on thick SiO_2/Si^+ substrates and then proceed with TEBAL to make structures with more complicated geometries, such as those presented in this paper, which are inaccessible with EBL only (e.g., Figure 1).

The EBL pre-patterned membrane device is then loaded onto a TEM device holder (Figure 2a) and entered into the low-pressure ($<10^{-8}$ Torr) chamber of a JEOL 2010F HRTEM at room temperature. The device is oriented on the holder such that the metallized side of the membrane faces away from and perpendicular to the beam source (i.e., it is face down). Using the standard imaging mode of the microscope with a ~5 Å diameter electron beam, accelerating voltage at 200 kV, minimum convergent beam angle (α3 mode on a JEOL 2010F), magnification typically below 100 000×, and the beam current density below ~10 pA/cm^2, the region of the initial metal to undergo TEBAL is located. Next, the magnification is increased to 800 000× (maximum magnification still visible on the fluorescent imaging screen), the beam is switched to maximum convergent beam angle (α1 mode), and is then condensed to its narrowest diameter (<1 nm) while situated slightly away (~10 nm) from the target region for optimizing the beam focus, alignment, and stigmation correction. Once optimized, the beam appears on the imaging screen as a small disk with a bright "caustic spot" at its center. The current density after optimization is ~50 pA/cm^2. Next, the beam is aimed at the desired pixels of the metal to be ablated. The user is actually able to see the ablating effect of the caustic spot on the metal in real time because of the low-intensity illumination of the beam surrounding this high-intensity center region. The time between exposing the metal to the condensed beam and the ablation is on the order of seconds, although the exact time required will depend on the metal being ablated and the microscope conditions. We observe that ablation is initiated more easily at points of high surface energy (e.g., the edge of a wire). Ablation is carried out until the desired pattern is made and is then stopped by reducing the beam current

density near the target material back to below ~10 pA/cm^2 either by moving the beam away from the target material or by leaving its position unchanged and reducing the intensity of the beam. For all of the metals that we have explored (Ag, Ni, Cr, Al, and Au), the ablation effect seems to stop almost immediately after the current density around the ablated area is reduced.

Prior to TEB exposure, the metal is amorphous/polycrystalline. High-resolution imaging of the TEBAL process reveals that high-intensity TEB exposure first anneals an exposed region into a crystalline domain and continued exposure drives the ablation of the newly formed lattice resulting in complete removal of the atoms from the surface. Figure S11 (Supporting Information) shows the TEB-induced transition of an amorphous Au island to a single crystal. Figure S12 (Supporting Information) shows the final stages of ablating a spot in a Ag film that has been locally annealed by brief exposure to the high-intensity TEB. Figure S12c shows that an ablated spot and the crystal lattice of the locally annealed surrounding region meet at a sharp edge. Additionally, we observe that the TEB anneals any grain boundaries in the metal films that it encounters. In practice, the size of the structures that can be made with TEBAL does not appear to be limited by grain size.

The TEB alters both the metal and the silicon nitride substrate. However, the rate at which metal is ablated (~10 nm^3/s) is much greater than the rate at which the substrate is affected, and in most cases, the changes in the nitride are negligible and not observable with TEM. While carving out the metal takes only a few seconds, it takes several minutes to drill a hole in a bare Si_3N_4 membrane with a 200 keV beam. The brighter (white) areas in some TEM images are regions where the TEB removed possible impurities from the surface, removed some of the nitride, or a combination of both.

Figure 3 shows an image gallery of additional metal nanostructures (nanowires, nanochannels and nanogaps) made with TEBAL on Si_3N_4 membranes. A ~40 nm long nanowire is shown at three stages of its formation by trimming down the two sides of a metal strip from ~60 to 12 nm (Figure 3a−c). Three additional examples of finished Ni/Cr nanowires with dimensions ~3.5 nm × 50 nm, 6 nm × 132 nm, and 13 nm × 61 nm are also shown (Figure 3d−f). Also shown is the fabrication of nanochannels ~3.1 to ~7.8 nm wide up to ~85 nm long (Figure 3g−k), a rodlike Ni nanoparticle ~15 nm × ~54 nm, made by carving out two nanochannels (Figure 3j−l), and a nanohole ~1.9 nm in diameter drilled in Cr (Figure 3m). Parts n−o of Figure 3 show two stages of carving out and "cleaning" debris from a ~5.2 nm large nanogap in Au. Specifically, Figure 3n shows a 13 nm wide constriction in Au and the Au nanoparticle debris on both sides of the constriction. These nanoparticles were removed as the silicon nitride surface was "cleaned" by ablation in Figure 3o while defining a clean nanogap. It is important to note that, while all other metals used in this work can be nanosculpted into arbitrary patterns, Au reacts differently to the TEB. Instead of being removed from the substrate during TEBAL, Au atoms crystallize into robust lattice domains. We exploited this property of Au to make the nanogap in Figure 3o (and the nanogaps in Figure 8). The fabrication works by encouraging the formation of crystallization sites on either side of the narrow neck of Au (Figure 3n) so that, upon sustained TEB exposure, the atoms leave the neck region in favor of being incorporated into the growing crystalline contacts, forming the nanogap in the process (see Figure S13, Supporting Information, for high-resolution images of the formation of a Au nanogap with crystalline contacts). This example illustrates the use of TEBAL to quickly "correct" and "clean" the EBL-made patterns, thus increasing the yield of the standard EBL process.

Illustrating the degree of control during the fabrication of an arbitrary pattern with sub-10 nm features, Figure 4 shows four steps toward making a pair of nanosculpted squares in a Ag film. These two neighboring squares are made by carving out seven line segments, ~50 nm long and from ~3.5 to ~10 nm wide, and leaving two ~12 nm long constrictions, thus defining two square-like metal islands connected to the parent material (detailed dimensions of each segment are shown in the Supporting Information). Importantly, this example demonstrates that, with TEBAL, lines can be formed in one direction and then suddenly redirected at a right angle.

The aspect ratios and geometries of these TEBAL-fabricated nanowires, nanogaps, and nanochannels illustrated in Figure 3 can be finely tuned with the electron beam, and this pattern control makes them particularly interesting for studies of superconductivity, molecular electronics, nanofluidics, and nanoparticle manipulation with electromagnetic fields. By running electrical currents through TEBAL-fabricated nanowires with tailored geometries, they can serve as nanomagnets for manipulation of nanoscale particles on a chip[38] and for cold neutral atom manipulation in vacuum above a chip on size scales at least 10−1000 times smaller than presently possible.[39−45] Certain nanowire patterns can be used to trap and guide particles in vacuum above a chip for applications in atom optics, coherent wavefunction propagation, and quantum information processing. Such wire patterns can generate magnetic fields (and also electric fields) that vary locally on a nanometer scale and whose spatial profile can be finely tuned by tailoring the wire shape. Even moderate (ac or dc) currents (~10 μA) in a nanometer-scale wire correspond to record large magnetic field gradients (forces) ~10^6 T/m and curvatures (frequencies) ~10^{15} T/m^2, estimated at the wire surface.

For device performance, it is important to ensure that TEBAL itself does not contaminate the fabricated devices. If a silicon nitride membrane surface is contaminated prior to being loaded into the TEM chamber, then the TEB will typically cause the outgassed contaminant to recondense onto the membrane surface along the TEB's perimeter, forming a ring. To avoid this situation, we let the recently EBL-processed devices outgas in ambient conditions overnight or clean them with O_2 plasma before doing TEBAL. Additionally, contaminants can also be removed after TEBAL with a brief exposure to O_2 plasma.

To demonstrate that TEBAL-fabricated devices are of high quality and contamination-free, we present current−voltage

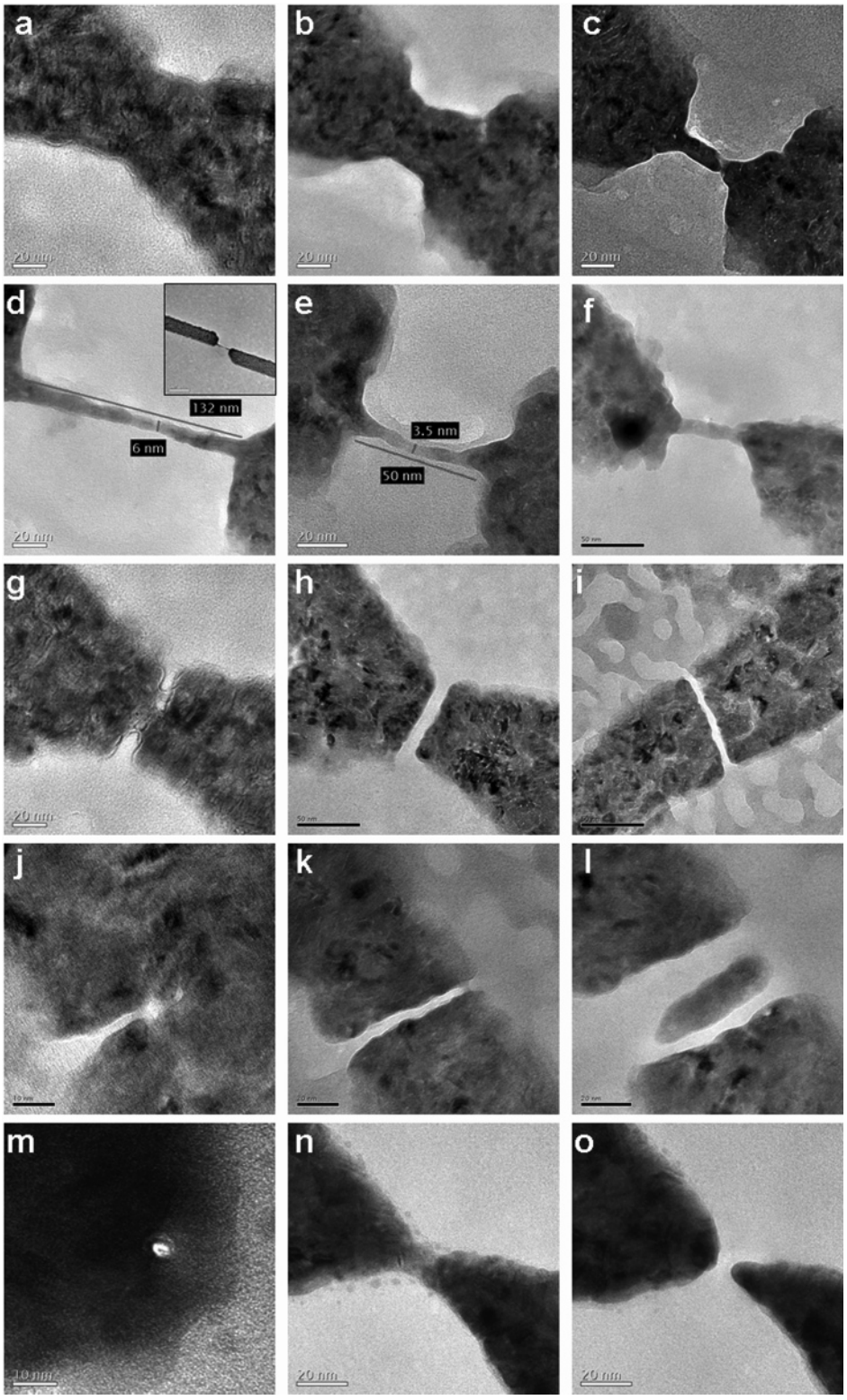

Figure 3. TEBAL example gallery. (a−c) TEBAL fabrication of a nanowire made of a Ni/Cr alloy (all scale bars = 20 nm). (d−f) Additional examples of Ni/Cr alloy nanowires. The width and length (W,L) of the nanowires in nm are (6,132), (3.5,50), and (13,61), respectively (scale bars = 20, 20, and 50 nm). (g) "Bottleneck" structure (scale bar = 20 nm). (h) Nanochannel ~7.8 nm wide (scale bar = 50 nm). (i) Nanochannel 3.1 nm wide, ~85 nm long (scale bar = 50 nm). (j−l) Three stages of "carving out" a Ni nanoparticle (all scale bars = 20 nm). (m) Nanohole ~1.9 nm diameter drilled into Cr (scale bar = 10 nm). (n,o) Au wire with narrow constriction before and after removing debris and making a clean 5.2 nm nanogap with TEBAL (scale bars = 20 nm).

($I-V$) measurements of a circuit that is *open* due to a TEBAL-made nanogap and one that is *closed* by a TEBAL-made nanowire. The measurements were conducted inside of a modified Janis ST-100H cryostat capable of achieving temperatures from 4 to 800 K. The devices were wired to a ceramic chip carrier thermally coupled to a copper cold finger

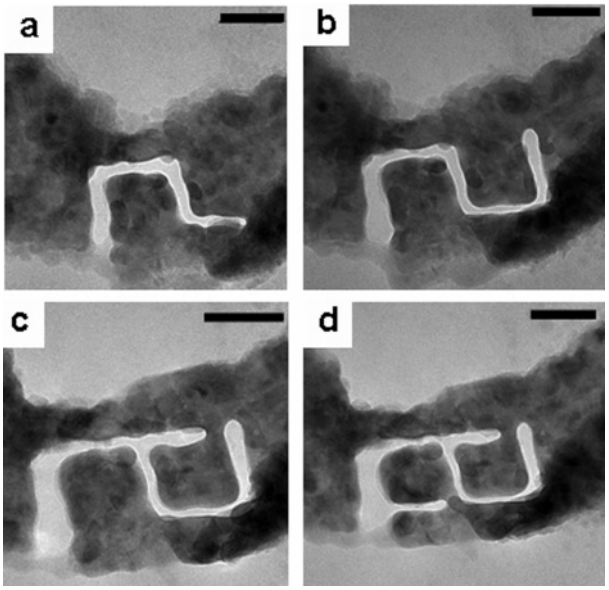

Figure 4. Four steps toward making a pair of squares in Ag. (a) First, features are composed of four joint line segments, each at right angles to its neighbor. (b) Addition of line segment at 90° to the right-most line segment. (c) Right square is defined and left connected to the parent material by a short nanowire. (d) Left square is defined and left connected to the parent material by a short nanowire. All scale bars = 50 nm.

and electrically addressed by silver-soldered wires, which coupled the source and drain pins to two independent BNC breakout boxes. Voltages were applied with a Yokogawa 7651 programmable dc source, and current signals were amplified and filtered by a vibrationally isolated Keithley 428 current amplifier and then measured with an Agilent 34401A 6 1/2 digital multimeter. Figure 5a shows the result of measurement of the ~3.5 nm wide by 50 nm long nanowire shown in the inset (and in Figure 3e). Two-terminal electrical characterization of this nanowire under vacuum (pressure $<10^{-6}$ Torr) from room temperature down to ~4 K displayed Ohmic resistance of ~30 kΩ. The resistance was insignificantly dependent on temperature, changing less than 1% over the measured range. Reduced sensitivity to temperature with reduced wire diameter has been reported by Natelson et al.,[46] where the smallest wire studied was ~5 nm. Our wire differs from these previous studies because of the absence of contact resistance to the leads, which may contribute to the role of temperature dependence. Additionally, the short length of this wire (~50 nm) makes it unlikely that postfabrication contacting would have been successful. Figure 5b shows the result of $I-V$ measurement of the ~2.5 nm nanogap shown in the inset (and in Figure 8c). The source−drain leakage current for this device was ~20 fA at 100 mV at 77 K. The current sensitivity of this device is therefore high, allowing the study of even highly insulating nanostructures. Considering that only the extremely small nanogap region of the surface need be contaminated in order to short the circuit, and that this region is where contamination is most likely to occur (i.e., where the TEB spends the most time during the fabrication), such a low current magnitude suggests that contamination from the TEM environment is negligible.

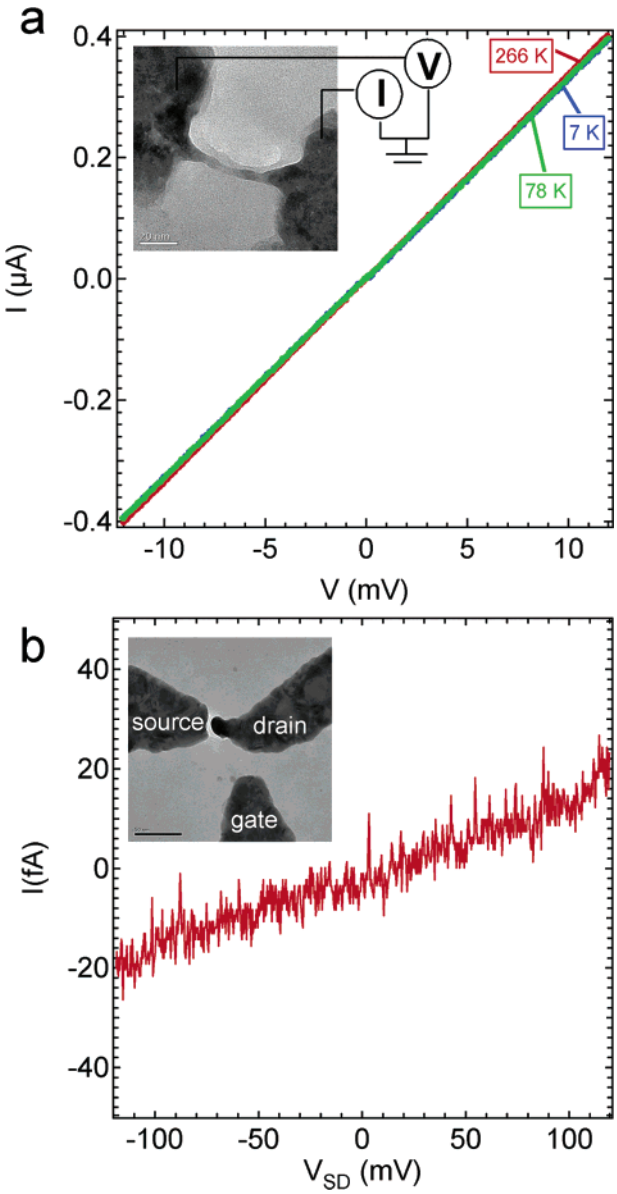

Figure 5. Device characterization (a) Current−voltage ($I-V$) measurements of 3.5 nm wide nanowire shown in Figure 3e. Data shown for measurement temperatures 266, 78, and 7 K. Inset: TEM image of the nanowire (scale = 20 nm). (b) Background source-drain current−voltage signal of the three-terminal NGFET shown in Figure 8c. Inset: TEM image of the device (scale = 50 nm).

The geometrical flexibility and the ease of electrical contacting makes the TEBAL-fabricated wires especially interesting for studying the effects of wire size and shape on conductivity in normal and superconducting wires. In Al nanowires, for example, superconductivity breaks down for wire widths below ~10 nm.[5] Tailoring wire shapes would allow the creation of modulated local regions of normal and superconducting behavior and in turn allow the creation of superconducting−normal (S−N) and superconducting−insulating (S−I) modulated wires for studies of quantum phase transitions.[2−6]

TEBAL is well suited for the fabrication of multi-terminal electronic devices where small, nanometer-scale separation between metal electrodes is required. In addition to a simple geometry with source and drain electrodes, more complicated

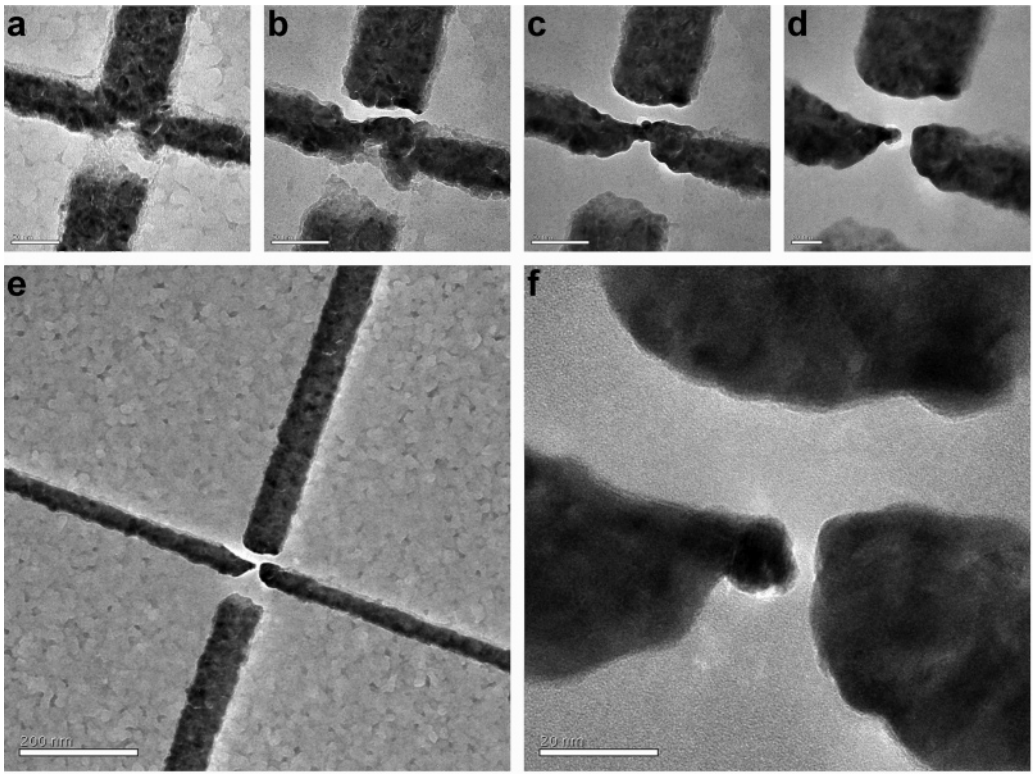

Figure 6. Making a four-terminal nanogap field effect transistor (NGFET) out of two intersecting Ag wires. (a−d) Ag is ablated until a nanogap is defined with gate electrodes on both of its sides (scale bars = 50, 50, 50, 20 nm, respectively). (e) Large-scale view of the completed four-terminal NGFET (scale bar = 200 nm). (f) Zoomed-in view of nanogap and upper gate electrode (scale bar = 20 nm).

geometries with multiple electrodes or nearby gate electrodes for local control can be easily fabricated with this technique. Fabrication can be also performed on the back side of the silicon nitride membranes to fabricate, for example, a global back gate. Examples of three-, four-, and eight-terminal devices are shown in Figures 6, 7, and 8. Figure 6a−d shows four steps in making a four-terminal nanogap field effect transistor (NGFET) out of two intersecting Ag lines. The final device consists of two electrodes forming a ∼2.3 nm large nanogap and two gate electrodes ∼19 and ∼56 nm away from the nanogap region.

Figure 7 shows an eight-terminal TEBAL-fabricated device consisting of eight Ni/Cr electrodes defined along a perimeter of a circle with radius ∼15 nm. The device was formed by cutting lines out of one continuous region. The cutting rate was ∼1 nm/s (in the direction of the line). The large number of electrodes allows this device to be used to generate a variety of electromagnetic fields for trapping and manipulating particles. Viewed another way, these electrodes form eight neighboring nanogaps, all within a ∼30 nm diameter region. As yet another application, a nanoscale object as small as ∼30 nm could be electrically characterized along different directions to investigate potential anisotropies.

Figure 8 shows three three-terminal devices, all fabricated with TEBAL on the same $\sim 50 \times 50\ \mu m^2$ membrane window (Figure 8e). Each device consists of a nanogap (∼1.5, 2, and 2.5 nm) and gate electrode (∼40 nm from each nanogap). Additionally, a nanohole has been drilled into the membrane exactly inside each of the nanogap regions (Figure S3, Supporting Information). This type of device may be used as a NGFET for a range of molecular electronic applications. Furthermore, this example demonstrates the reproducibility of TEBAL fabrication *by hand*.

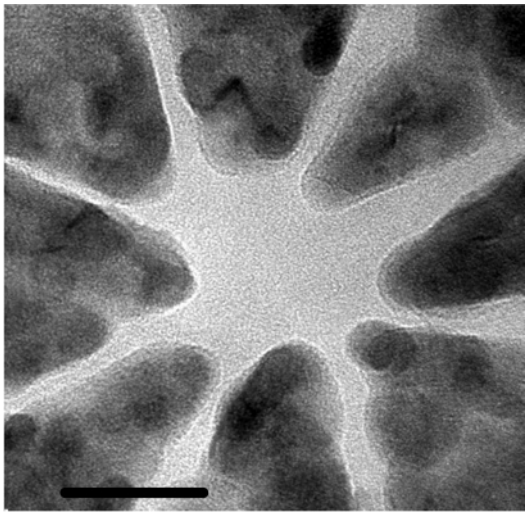

Figure 7. Eight-terminal device fabricated from Ni/Cr (scale bar = 20 nm).

Several groups have demonstrated the fabrication of nanoholes in insulating membranes by using TEBs[19−21] and focused ion beams (FIBs).[47] Nanoholes have been useful for manufacturing single-molecule detectors and have been used to study translocation of DNA molecules[48−53] and carbon nanotubes[54] by measuring ionic current between macroscopic electrodes as molecules pass through the nanohole. These and other advancements suggest possible applications of nanoholes to DNA size determination and sequencing. As

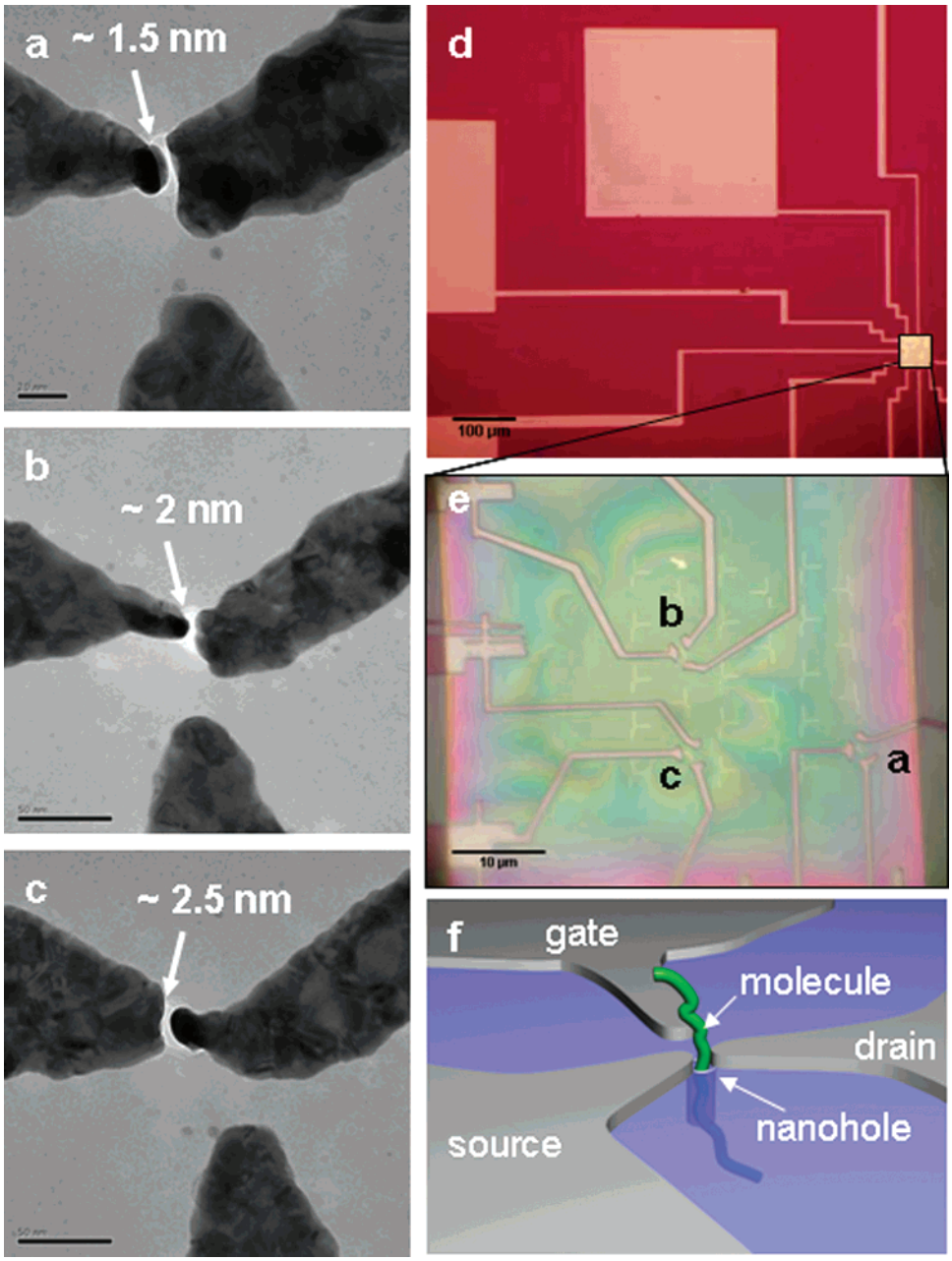

Figure 8. Devices for molecular detection and analysis. (a−c) Source, drain, and gate devices with nanohole for molecular translocation (scale bars = 20, 50, and 50 nm, respectively). (d) Optical micrograph of the full device containing the three molecular "analyzers". The membrane window is seen in the lower right corner and has wires running from it out to large contact pads (scale bar = 100 μm). (e) Optical micrograph of the membrane window showing the three analyzers (a−c) connected to leads (scale bar = 10 μm). (f) Schematic illustrating vertical translocation of a molecule through the nanohole while being probed with the source, drain, and gate electrodes.

mentioned above, the devices we show in Figure 8 each have a nanohole spanning their nanogap. (Zoom-in view of the nanohole region is shown in Figure S3). By applying a potential difference across these electrodes, electrical current (or capacitance) could be monitored to characterize a molecule during its translocation through the nanohole (illustrated in Figure 8f). Lagerqvist et al.[55] have recently performed molecular dynamics and quantum-mechanical current calculations for this situation and calculate the difference in electrical current signals of different base pairs to be rather large, of the order of 0.1 nA. Depending on the electrode thickness, a smaller or larger fraction of a molecule such as DNA could be electrically characterized. The thickness of metal electrodes can be reduced by ablation with subnanometer precision. This could further increase the sensitivity and lower the detection limit of these devices. However promising, the feasibility of this approach will be ultimately determined by future biophysics experiments.

All of the structures in this letter were prepared "by hand" in the sense that a human user shifted the beam while watching the ablation in real time. Computer control should offer an even higher degree of precision than what has been demonstrated here and can therefore produce highly intricate patterns over a wide membrane area. Computerized automation is possible by measuring the current density of the beam (Figure 2a) during TEBAL. Once the current density of the

beam is measured on an unmetallized region of the membrane, later comparisons of real-time values to this reference value are used to inform the computer of whether or not the beam is on or off a metal region. This fact can be used to have the automated system find the metal regions on the membrane. By running into the metal several times with slight displacements, the system finds an axis parallel to the metal edge and can carry out ablation with respect to this known axis.

In conclusion, we have demonstrated the precision, versatility, and reproducibility of metal nanosculpting by controlled atom ablation via the imaging beam of a HRTEM for the manufacturing of ultrasmall metal devices on insulating silicon nitride membranes. The applications of TEBAL include the areas of nanoelectronics, superconductivity, molecular translocation, nanofluidics, and atom/nanoparticle manipulation with highly localized electromagnetic fields. TEBAL is expected to work on a wider class of materials than has been demonstrated here and, as an example, may provide a method for nanosculpting graphene. Future work involving simultaneous in situ fabrication and measurement of test structures may provide additional insight to the mechanisms at work during TEBAL in addition to revealing fundamental science of the fabricated structures.

Acknowledgment. This work has been supported by the NSF Career Award DMR-0449533, NSF MRSEC DMR05-20020, and ONR award YIPN000140410489. M.F. acknowledges funding from the NSF-IGERT program (grant DGE-0221664).

Supporting Information Available: Schematic of Si_3N_4 membrane window device; fabrication of nanoring shown in Figure 1a; larger view of device in Figure 8c showing the nanohole in the nanogap; quantitative analysis of the TEM images shown in Figures 1−4, and 6−8, obtained with ImageJ software; high-resolution TEM images of TEB-induced local amorphous to crystalline transition and lattice ablation; high-resolution TEM images of Au nanogap formation with crystalline contacts. This material is available free of charge via the Internet at http://pubs.acs.org.

References

(1) Werner, W. S. M.; Tomastik, C.; Cabela, T.; Richter, G.; Störi, H. *Surf. Sci*. **2000**, *470*, L123.
(2) Gurney, B. A.; Speriosu, V. S.; Nozieres, J.-P.; Lefakis, H.; Wilhoit, D. R.; Need, O. U. *Phys. Rev. Lett*. **1993**, *13*, 4023.
(3) Bezryadin, A.; Lau, C. N.; Tinkham, M. *Nature* **2000**, *404*, 971.
(4) Lau, C. N.; Markovic, N.; Bockrath, M.; Bezryadin, A.; Tinkham, M. *Phys. Rev. Lett*. **2001**, *87*, 217003.
(5) Zgirski, M.; Riikonen, K.-P.; Toubloltsev, V.; Arutyunov, K. *Nano Lett*. **2005**, *5*, 1029.
(6) Beenakker, C. W. J.; van Houten, H. *Phys. Rev. Lett*. **1991**, *66*, 3056.
(7) Tas, N. R.; Haneveld, J.; Jansen, H. V.; Elwenspoek, M.; van den Berg, A. *Appl. Phys. Lett.* **2004**, *85*, 3274.
(8) Tan, H.-S.; Piletic, I. R.; Riter, R. E.; Levinger, N. E.; Fayer, M. D. *Phys. Rev. Lett*. **2005**, *94*, 057405.
(9) Austin, R. H.; Tegenfeldt, J. O.; Cao, H.; Chou, S. Y.; Cox, E. C. *IEEE Trans. Nanotechnol*. **2002**, *1*, 12.
(10) Cherns, D *Philos. Mag.* **1977**, *36*, 1429.
(11) Cherns, D. *Surf. Sci.* **1979**, *70*, 339.
(12) Cherns, D.; Hutchison, J. L.; Jenkins, M. L.; Hirsch, P. B. *Nature* **1980**, *287*, 314.
(13) Isaacson, M.; Murray, A. *J. Vac. Sci. Technol.* **1981**, *19*, 1117.
(14) Mochel, M. E.; Eades, J. A.; Metzger, M.; Meyer, J. I.; Mochel, J. M. *Appl. Phys. Lett.* **1984**, *44*, 502.
(15) Mochel, M. E.; Humphreys, C. J.; Eades, J. A.; Mochel, J. M.; Petford, A. M. *Appl. Phys. Lett.* **1983**, *42*, 392.
(16) Salisbury, I. G.; Timsit, R. S.; Berger, S. D.; Humphreys, C. J. *Appl. Phys. Lett.* **1984**, *45*, 1289.
(17) Takeda, S.; Koto, K.; Iijima, S.; Ichihashi, T. *Phys. Rev. Lett*. **1997**, *79*, 2994.
(18) Bysakh, S.; Shimojo, M.; Mitsuishi, K.; Furuya, K. *J. Vac. Sci. Technol., B* **2004**, *22*, 2620.
(19) Storm, A. J.; Chen, J. H.; Ling, X. S.; Zandbergen, H. W.; Dekker, C. *Nat. Mater*. **2003**, *2*, 537.
(20) Heng, J. B.; Ho, C.; Kim, T.; Timp, R.; Aksimentiev, A.; Grinkova, Y. V.; Sligar, S.; Schulten, K.; Timp, G. *Biophys. J*. **2004**, *87*, 2905.
(21) Wu, M.-Y.; Krapf, D.; Zandbergen, M.; Zandbergen, H.; Batson, P. E. *Appl. Phys. Lett.* **2005**, *87*, 1131061.
(22) Kizuka, T. *Phys. Rev. Lett*. **1998**, *81*, 4448.
(23) Iijima, S.; Ichihashi, T. *Phys. Rev. Lett*. **1986**, *56*, 616.
(24) Kondo, Y.; Takayanagi, K. *Phys. Rev. Lett.* **1997**, *79*, 3455.
(25) Lee, J.-G.; Lee, J.; Tanaka, T.; Mori, H. *Phys. Rev. Lett.* **2006**, *96*, 075504.
(26) Yokota, T. Murayama, M.; Howe, J. M. *Phys. Rev. Lett*. **2003**, *91*, 265504.
(27) Hiraki, J.; Mori, H.; Taguchi, E.; Yasuda, H.; Kinoshita, H.; Ohmae, N. *App. Phys. Lett.* **2005**, *86*, 223101.
(28) Chen, G. S.; Boothroyd, C. B.; Humphreys, C. J. *Appl. Phys. Lett*. **1993**, *62*,1949.
(29) Zandbergen, H. W.; van Duuren, R. J. A.; Alkemade, P. F. A.; Lientschnig, G.; Vasquez, O.; Dekker, C.; Tichelaar, F. D. *Nano Lett*. **2005**, *5*, 549.
(30) Terrones, M.; Banhart, F.; Grobert, N.; Charlier, J.-C.; Terrones, H.; Ajayan, P. M. *Phys. Rev. Lett.* **2002**, *89*, 075505.
(31) Xu, S.; Tian, M.; Wang, J.; Xu, J.; Redwing, J. M.; Chan, M. H. W. *Small* **2005**, *1*, 1221.
(32) Remeika, M.; Bezryadin, A. *Nanotechnology* **2005**, *16*, 1172.
(33) Grant, A. W.; Hu, Q.-H.; Kasemo, B. *Nanotechnology* **2004**, *15*, 1175.
(34) Si_3N_4 membranes are an excellent platform for device manufacturing; they have a dielectric constant of ∼6.5−7.2 and a breakdown voltage of $\sim 10^7$ V/cm, making them an attractive alternative dielectric material compared to SiO_2.[35]
(35) Ma, T. P *IEEE Trans. Electron. Devices* **1998**, *45*, 680.
(36) Broers, A.N. *IBM. J. Res. Dev.* **1998**, *32*, 502.
(37) Fischbein, M. D.; Drndić, M. *Appl. Phys. Lett*. **2006**, *88*, 063116.
(38) Lee, C. S.; Lee, H.;Westervelt, R. M. *Appl. Phys. Lett.* **2001**, *79*, 3308.
(39) Drndic, M.; Johnson, K. S.; Thywissen, J. H.; Prentiss, M.; Westervelt, R. M. *Appl. Phys. Lett.* **1998**, *72*, 2906.
(40) Reichel, J. *Sci. Am.* **2005**, *262*, 46.
(41) Leanhardt, A. E.; Shin, Y.; Chikkatur, A. P.; Kielpinski, D.; Ketterle, W. *Phys. Rev. Lett.* **2003**, *90*, 100404.
(42) Dekker, N. H.; Lee, C. S.; Lorent, V.; Thywissen, J. H.; Smith, S. P.; Drndic, M.; Westervelt, R. M.; Prentiss, M. *Phys. Rev. Lett*. **2000**, *84*, 1124.
(43) Ott, H.; Fortagh, J.; Schlotterbeck, G.; Grossmann, A.; Zimmermann, C. *Phys. Rev. Lett.* **2001**, *87*, 230401.
(44) Hansel, W.; Hommelhoff, P.; Hansch, T. W.; Reichel, J. *Nature* **2001**, *413*, 498.
(45) Schumm, T.; Hofferberth, S.; Andersson, L. M.; Wildermuth, W.; Groth, S.; Bar-Joseph, I.; Schmiedmayer, J.; Kureger, P. *Nat. Phys.* **2005**, *1*, 57.
(46) Natelson, D.; Willet, R. L.; West, K. W.; Pfeiffer, L. N. *Solid-State Commun*. **2000**, *115*, 269.
(47) Li, J.; Stein, D.; McMullan, D.; Branton, E.; Aziz, M. J.; Golovchenko, J. A. *Nature* **2001**, *412*, 166.
(48) Bezrukov, S. M.; Vodyanoy, I.; Parsegian, V. A. *Nature* **2004**, *370*, 279.
(49) Meller, A.; Nivon, L.; Branton, D. *Phys. Rev. Lett.* **2001**, *86*, 3435.
(50) Li, J.; Gershow, M.; Stein, D.; Brandin, E.; Golovchenko, J. A. *Nat. Mater*. **2003**, *2*, 611.
(51) Kasianowicz, J. J.; Brandin, E.; Branton, D.; Deamer, D. W. *Proc. Natl. Acad. Sci. U.S.A.* **1996**, *93*, 13770.
(52) Storm, A. J.; Storm, C.; Chen, J.; Zandbergen, H.; Joanny, J.-F.; Dekker, C. *Nano Lett.* **2005**, *5*, 1193.
(53) Vercoutere, W.; Winters-Hilt, S.; Olsen, H.; Deamer, D.; Haussler, D.; Akeson, M. *Nat. Biotechnol*. **2001**, *19*, 248.
(54) King, G. M.; Golovchenko, J. A. *Phys. Rev. Lett.* **2005**, *95*, 2161031.
(55) Lagerqvist, J.; Zwolak, M.; Di Ventra, M. *Nano Lett.* **2006**, *6*, 779.

NL0703626